Article

Characterization and Reactivity of MnO Supported on Mesoporous Zirconia for Herbicide 2,4-D Mineralization with Ozone

Shengtao Xing, Chun Hu, Jiuhui Qu, Hong He, and Min Yang

Environ. Sci. Technol., **2008**, 42 (9), 3363-3368 • DOI: 10.1021/es0718671 • Publication Date (Web): 30 November 2007

Characterization and Reactivity of MnO_x Supported on Mesoporous Zirconia for Herbicide 2,4-D Mineralization with Ozone

SHENGTAO XING, CHUN HU,* JIUHUI QU,* HONG HE, AND MIN YANG

State Key Laboratory of Environmental Aquatic Chemistry, Research Center for Eco-Environmental Sciences, Chinese Academy of Sciences, Beijing 100085, China

Received July 26, 2007. Revised manuscript received September 19, 2007. Accepted September 24, 2007.

Manganese oxide was supported on mesoporous zirconia (MnO_x/MZIW) by wet impregnation, drying, water washing, and calcinations with manganese acetate tetrahydrate as the metal precursor for the first time and was characterized by X-ray diffraction (XRD), X-ray photoelectron spectroscopy (XPS), Fourier-transform infrared spectra (FTIR), temperature-programmed reduction (TPR), temperature-programmed oxygen desorption (O_2—TPD), and UV–vis diffuse reflectance spectra (UV–vis DRS) measurements. The catalyst was found to be highly effective for the mineralization of 2,4-dichlorophenoxyacetic acid (2,4-D) aqueous solution with ozone. The characterization studies showed that nonstoichiometrically MnO_x was highly dispersed on mesoporous zirconia by the strong interaction of the $[Mn(H_2O)_6]^{2+}$ complex with surface hydroxyls of the support. Moreover, the multivalence oxidation states of MnO_x enhanced the electron transfer, causing the higher catalytic reactivity. On the basis of all information obtained under different experimental conditions, MnO_x/MZIW enhanced the mineralization of 2,4-D by the formation of $^{\bullet}OH$ radicals resulting from the catalytic decomposition of ozone.

Introduction

Heterogeneous catalytic ozonation has received increasing attention in recent years because of its potentially higher effectiveness in the degradation and mineralization of refractory organic pollutants and lower negative effect on water quality. It has been developed to overcome the limitations of ozonation processes, such as the formation of byproducts and selective reactions of ozone, which are designed to enhance the production of hydroxyl radicals ($^{\bullet}OH$), known nonselective oxidants (*1, 2*). Specifically, metal oxides are more practical in catalytic ozonation than ionized metals because metal oxides hinder bromate formation in the reaction with ozone and are less pH-sensitive than ionized metals (*3, 4*).

So far, metal oxides (e.g., MnO_2, TiO_2, and Al_2O_3), metal oxides on supports, and activated carbons have been proposed as effective catalysts for ozonation processes (*5–7*). Among these, Mn oxide (MnO_x) was reported to have a higher ozone decomposition rate than Co, Ni, Cr, Ag, Cu, Ce, Fe, V, and Mo oxides (*8, 9*). Moreover, MnO_x supported on silica and Al_2O_3 are complete oxidation catalysts for the elimination of volatile organic compounds in air (*10*). However, these catalysts have not yet been applied much for the catalytic ozonation of organic pollutants in water.

The catalytic activity of metal oxide depends on the size distribution and morphology of particles. It is evident that enormously increased numbers of active sites would be present on the surface of smaller particles for a given amount of catalyst material. Hence, reduction of the diameter of heterogeneous catalysts to nanometer scale may result in enhanced reactivity of the heterogeneous catalysts at a given amount (*11*). Presently, MnO_x nanocrystals with various morphologies have been obtained, using porous materials as solid nanoreactors, by a method called "nanocasting". Generally, inorganic precursors are first introduced into channels of host materials such as mesoporous silicas. Then, MnO_x nanocrystals are produced with a replica of the confined space by subsequent calcinations. Because of the facile phase transformation of MnO_x during preparation, only multivalent mixtures of manganese oxides are usually obtained. To date, direct synthesis of MnO_x with a defined crystalline structure in nanoreactors is still far from easy. However, supported MnO_x nanoparticles can be produced by impregnation and thermolysis. Nanoparticles of MnO_x supported on mesoporous silica SBA-15 have been obtained by high dispersion (*12*). The structure and dispersion of the supported metal oxide depend primarily on the preparation method, the nature of the support, and the type of precursor. Ordered mesoporous materials, with their intrinsically high surface areas, are particularly suitable for this purpose.

In the present study, for the first time, MnO_x nanoparticles were highly dispersed on the surface and channels of ordered mesoporous zirconia by the impregnation of the acetate precursor solution, followed by drying at 383 K, washing with water, and calcining at 573–773 K. This was attributed to the strong interaction of the $[Mn(H_2O)_6]^{2+}$ complex with surface hydroxyls of the MZ (*13*) and the ordered mesoporous structure of MZ on the basis of different experimental information. 2,4-Dichlorophenoxyacetic acid (2,4-D) is the most widely used herbicide in the world (*14*). It is poorly biodegradable and has been detected as a major pollutant in ground and surface waters. Most papers related to the treatment of chlorophenoxy herbicides in aqueous medium describe the degradation of 2,4-D by advanced oxidation processes (AOPs) involving chemical (*15*), photochemical (*16*), or photocatalytic (*17*) production of hydroxyl radicals. In these processes, the mineralization of 2,4-D needed a prolonged reaction time. Catalytic ozonation has great potential for the mineralization of the refractory organics. Therefore, 2,4-D was selected to evaluate the activity and properties of the catalyst with ozone in aqueous solution. The results indicated that the catalyst exhibited higher reactivity for the catalytic ozonation of 2,4-D. A preliminary effort to identify a correlation between the surface properties of supported MnO_x compounds and their catalytic activity has been undertaken.

Experimental Section

Materials and Reagents. All reagents used in this work were analytical grade and were used without further purification. Zirconium oxychloride, manganese acetate tetrahydrate, and 2,4-D were purchased from the Yili Company. Triblock copolymer $(EO)_{20}(PO)_{70}(EO)_{20}$ (P123) was purchased from Sigma-Aldrich. All solutions were prepared with deionized water.

Catalyst Preparation. Mesoporous zirconia (MZ) was prepared via solid-state reaction using the structure-directing

* Corresponding author phone: +86-10-62849628; fax: +86-10-62923541; e-mail: huchun@rcees.ac.cn(H.C); jhqu@rcees.ac.cn (Q.J).

10.1021/es0718671 CCC: $40.75
Published on Web 11/30/2007

method (*18*). Then MnO_x compounds were supported on MZ by the incipient wetness impregnation method with $[Mn(CH_3COO)_2 \cdot 4H_2O]$ as the metal precursor. As an example, 0.63 g of manganese acetate tetrahydrate was dissolved in 1 cm^3 of distilled water, and to this solution was then added 2 g of mesoporous zirconia (MZ). After impregnation, the sample was dried at 383 K for several hours, then cooled, and washed with 1 L of deionized water. The sample was dried at 383 K for several hours and finally calcined in a muffle furnace (exposed to static air) at 623 K for 2 h at a heating rate of 0.083 deg/s (5 deg/min). Following this procedure, the catalysts with different Mn content were prepared from 1 to 7 wt %. The catalyst with 5 wt % Mn exhibited the highest activity (Figure S1, Supporting Information); designated MnO_x/MZIW, and was used for all of the experiments. As reference, 5 wt% Mn supported on mesoporous zirconia or commercial ZrO_2 (CZ) were prepared in the manner described above without the water washing, and these compounds were designated MnO_x/MZI and MnO_x/CZI.

Characterization. Nitrogen adsorption/desorption experiments of MZ were carried out using a Micromeritics ASAP2000 analyzer (Micromeritics Co., U.S.A.). Powder X-ray diffraction of the catalyst was recorded on a Scintag-XDS-2000 diffractometer with Cu Kα radiation ($\lambda = 1.54059$ Å). UV–vis absorption spectra of the samples were recorded on a UV–vis spectrophotometer (Hitachi UV-3100) with an integrating sphere attachment and a reflectance standard of $BaSO_4$. The XPS data were taken on an AXIS-Ultra instrument from Kratos using monochromatic Al Kα radiation (225 W, 15 mA, 15 kV). The infrared spectrum of the dry samples supported on KBr pellets was recorded on a Nicolet FTIR spectrophotometer. The ζ potential of catalysts in KNO_3 (10^{-3} M) solution were measured with a Zetasizer 2000 (Malvern Co., U.K.) with three consistent readings. The experiments using O_2−TPD and TPR are described in the Supporting Information.

Procedures and Analysis. Batch experiments were carried out with a 1.2 L reactor. The reaction temperature was maintained at 20 °C. In a typical experiment, aqueous suspensions of 2,4-D (1 L, 80 mg/L) and 1.5 g of catalyst powder were placed in the reactor. The solution was continuously magnetically stirred, and 30 mg of gaseous O_3/L oxygen-ozone was bubbled into the reactor through the porous plate of the reactor bottom at a 12 L/h flow rate. The ozone was generated by a laboratory ozonizer (DHX-SS-IG, Harbin Jiujiu Electrochemistry Technology Co., Ltd., China) and pumped into the reactor. At given time intervals, samples were withdrawn and filtered through a Millipore filter (pore size 0.45 μm) for analysis. An aliquot of 0.1 M $Na_2S_2O_3$ was subsequently added to the sample to quench the aqueous ozone remaining in the reaction solution. The concentration of ozone dissolved in the aqueous phase was determined with the indigo method. 2,4-D was measured by high-performance liquid chromatography (HPLC, Alliance 2695) with an Xterra C18 column; 60% acetonitrite with water was used as the mobile phase. The total organic carbon (TOC) of the solution was analyzed with a Phoenix 8000 TOC analyzer. GC-MS analysis was carried out on an Agilent 6890GC/5973MSD with a DB-5 MS capillary column. The preparation of samples for GC-MS analyses is described in the Supporting Information.

Results and Discussion

XRD and N_2 Adsorption. The low-angle XRD patterns of MZ and MnO_x/MZIW are shown in Figure 1. The low-angle XRD pattern of the MZ sample showed a broader primary diffraction peak, indicating that the prepared MZ had an ordered mesostructure (*19*). The inorganic framework was periodic because it consisted of nanocrystallites in the tetragonal phase according to the XRD peaks at high angles

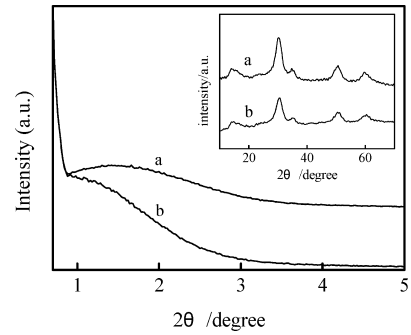

FIGURE 1. XRD patterns of different catalysts: (a) MZ and (b) MnO_x/MZIW. The inset shows the high-angle peak.

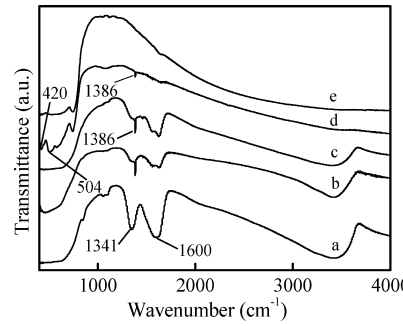

FIGURE 2. FTIR spectra of different samples: (a) MZ, (b) MnO_x/MZI, (c) MnO_x/MZIW, (d) MnO_x/ CZI, and (e) CZ.

shown in the inset of Figure 1. No XRD diffraction peaks of MnO_x species were observed in the sample at high angles. The XRD diffraction peaks of the MnO_x species were also not observed in MnO_x/MZI and MnO_x/CZI (Figure S2, Supporting Information). After the introduction of MnO_x, its low-angle XRD peaks shifted toward higher angles, although MZ still had a periodic mesoporous framework. This was attributed to the formation of MnO_x nanoparticles in the pores. In general, the introduction of scattering material into the pores leads to an increased phase cancelation between scattering from the wall and the pore regions and therefore to reduced scattering intensities for the Bragg reflections (*20*).

The N_2 adsorption–desorption isotherms are presented in Figure S3 (Supporting Information). MZ, MnO_x/MZIW, and MnO_x/MZI exhibited adsorption–desorption isotherms of type IV with hysteresis loops, which means that the materials had a mesoporous structure. The introduction of MnO_x did not change the distribution of the pore diameters (Figure S4, Supporting Information) and the BET surface area of MZ (232 m^2/g), indicating the high dispersion of MnO_x. As a reference, CZ also was characterized by N_2 adsorption–desorption. Its BET surface area was 8.83 m^2/g, and no mesopores were detected.

FTIR. The surface properties of the catalyst are very important for the degradation of organic pollutants in heterogeneous catalytic ozonation (*21*). Therefore, different catalysts were further characterized with FTIR. As shown in Figure 2 for MZ (Figure 2a), there were three OH absorption bands: the first one was at 3500–3200 cm^{-1}, corresponding to the stretching of OH groups of adsorbed water. The second one at 1600 cm^{-1} was assigned to the bending vibration of adsorbed water (*22*). The third one was at 1341 cm^{-1} and was attributed to the deformation vibration of Zr−OH (*23*). MnO_x/MZI and MnO_x/MZIW exhibited similar FTIR spectra to the MZ except for a new absorption peak at 1386 cm^{-1}, assigned to OH deformation vibrations of hydrated MnO_x (Figure 2b−c). In contrast, there were no OH groups on CZ (Figure 2e), except bands corresponding to weak OH stretching vibration (3400 cm^{-1}). MnO_x/CZI also exhibited a peak at

1386 cm^{-1}, assigned to OH deformation vibrations of hydrated MnO_x.Meanwhile, two weaker absorption peaks at 504 and 420 cm^{-1} appeared, which were consistent with those reported in the literature for Mn_3O_4 (*24*). The results indicated that MnO_x was not dispersed very well on CZ and that the MnO_x mainly existed as multivalence mixtures when produced by this synthesis method. On the basis of the FTIR analysis, the abundant surface hydroxyl of MZ led to higher dispersion of MnO_x than CZ.

XPS and UV–vis DRS Analysis. The dispersion of MnO_x on different samples was further studied by the distribution of Mn. The Mn concentrations on the whole-particle and the surface of the particle were measured by the analysis of XPS and ICP. Table S1 (Supporting Information) summarizes the analysis results for different samples. The Mn concentration on the surface phase (2.81 wt %) was much lower than that (4.92 wt %) in the bulk for MnO_x/MZIW. This result indicated that most of the manganese oxides were dispersed into the pore channels, while this phenomenon did not occur in the procedure of just impregnation and calcinations without water washing. The surface Mn concentration (5.71 wt%) was slightly lower than that (6.28 wt%) in bulk for MnO_x/MZI. These results revealed that MnO_x diffused into the pore channel of MZ because of the water washing, resulting in little manganese oxide being dispersed on the surface of MZ. In contrast, most of the MnO_x was loaded on the surface of CZ by impregnation and calcination; the surface Mn concentration (21.8 wt %) was much higher than that in the bulk (6.32 wt %). This was attributed to nonporosity, a smaller surface area, and most importantly, to insufficient surface hydroxyls of CZ. To verify this point, MnO_x supported on CZ also was prepared by impregnating, drying, washing with water, and then calcining. It was found that little manganese was loaded on the surface of CZ and that the dosages of Mn were almost completely washed out with water. By the same method, the dosages of Mn were almost completely loaded on MZ. These results suggested that the rich surface hydroxyl groups of MZ played an important role in the loading of MnO_x. These phenomena indicated that MnO_x was anchored on the surface of MZ by the interaction of $[Mn(H_2O)_6]^{2+}$ with the surface hydroxyls of the support. The UV–vis spectra of the precursor $Mn(CH_3COO)_2 \cdot 4H_2O$ aqueous solution exactly matched the published spectra of the $[Mn(H_2O)_6]^{2+}$ complex (*25*) (Figure S5, Supporting Information). This result confirmed that the $[Mn(H_2O)_6]^{2+}$ complex was the precursor molecule present in aqueous solution of manganese acetate. During the impregnation and the subsequent drying in air, the complex reacted with both the acidic and basic hydroxyls of MZ to form the linking $(H_2O)_xMn^{2+/3+}-O-Zr$. Then further oxidation of the manganese occurred by calcination. Thus, the dispersion of hydrated MnO_x depended on the distribution of the surface hydroxyl groups of MZ (MnO_x/MZI). In another preparation method, the sample was washed with water after it had been dried at 110 °C in air, causing some of the complex to be further diffused into the pore channels. Finally, MnO_x was obtained by calcination of MnO_x/MZIW. Therefore, by the latter method, the higher dispersion of MnO_x on MZ was attributed to the fixing role of surface hydroxyls and the diffusing role of water. Both MnO_x/MZI and MnO_x/CZI were black, while MnO_x/MZIW was pink. These phenomena indicated that MnO_x/MZIW still contained adsorbed water after calcinations at 623 K, while MnO_x/MZI and MnO_x/CZI mainly contained MnO_x. To affirm the metallic state of the manganese incorporated in these samples, these samples were characterized by XPS and UV–vis DRS. The Mn $2p_{3/2}$ binding energy values (BE) were in the range of 641.8 and 642.1 eV for the three catalysts (Figure S6, Supporting Information). The variation of XPS binding energies of Mn 2p alone, from Mn^{2+} to Mn^{4+}, usually is too small (less than ~1.0 eV) to precisely evaluate the Mn valence

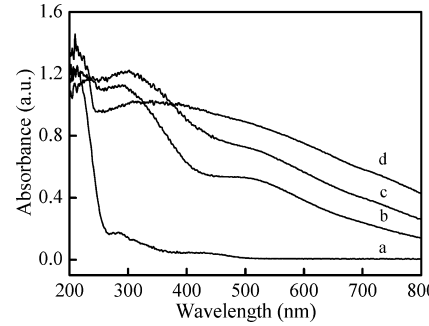

FIGURE 3. UV–vis diffuse reflectance spectra of different samples: (a) MZ, (b) MnO_x/MZIW, (c) MnO_x/MZI, and (d) MnO_x/CZI.

of MnO_x. However, it was found that the Mn2p XPS BE for supported MnO_x was higher than those for the pure bulk MnO_x by ~0.6–0.8 eV (*12, 26, 27*). Therefore, the Mn($2p_{3/2}$) BE in the range of 641.8 and 642.1 eV were attributed to $Mn^{2+/3+}$ oxidation states (*27*). Since UV–vis DRS can provide information regarding the oxidation state of manganese and its chemical environment, the diffuse reflectance UV–vis spectra of different samples are shown in Figure 3. The pure MZ spectrum only shows a strong absorption edge with a maximum at about 210 nm (curve a), which is attributed to charge transfer transitions from the 2p level of O to the 4d level of 8- or 7-fold coordinated Zr^{4+} (*24*). Both MnO_x/MZIW and MnO_x/MZI exhibited similar UV–vis spectra (curves b and c). An absorption band in the 250–315 nm range was observed, which could be reasonably assigned to $O^{2-} \rightarrow Mn^{2+}$ and $O^{2-} \rightarrow Mn^{3+}$ charge-transfer transitions in the hausmannite structure (*24*). Another broadband in the 430–505 nm region also appeared, attributed to the d−d transitions of Mn^{3+} and Mn^{4+} (*28*). The spectra of MnO_x/CZI displayed a continuous absorption from 250 nm to the visible region with a maximum at 350 nm (curve d). The band at 250 nm proved the presence of Mn^{2+} ions, whereas the continuous absorption in the visible region was related to the d → d charge transfer transitions of the Mn^{3+} cation (*24*). The different spectra of MnO_x/MZ and MnO_x/CZI may have been influenced by the support.

TPR and TPD. The H_2−TPR profiles of different catalysts are shown in Figure 4A. In the TPR curves of MnO_x/MZIW, MnO_x/MZI, and MnO_x/CZI, two peaks were observed. The peak at the lower temperature range, between 200 and 400 °C, can be attributed to the unresolved reduction peaks of nonstoichiometrically dispersed MnO_x ($1.5 < x < 2$) phase (reduced in the temperature range between 200 and 325 °C) (*29, 30*) and dispersed Mn_2O_3 (reduced at about 350 °C) (*29, 31, 32*). For MnO_x/MZIW, the lower reduced temperature is about 292 °C, indicating the existence of dispersed MnO_x. In both MnO_x/MZI and MnO_x/CZI, the lower reduced temperatures are about 344 and 354 °C, indicating the existence of dispersed Mn_2O_3. From the above results, it can be seen that there is a strong interaction between Mn species and MZ in MnO_x/MZIW. Such interaction led to the formation of the nonstoichiometrically dispersed MnO_x phase. For the three samples, the second peak at higher temperature, >400 °C, is attributed to the reduction of Mn_3O_4 to MnO (*33*). Figure 4B shows the O_2−TPD−MS spectra of the three samples. In the case of MnO_x/MZIW, a strong feature peak was observed at 450 °C, which was assigned to conversion of nonstoichiometric MnO_x species to Mn_2O_3 (*30*), and two weaker features also appeared at 520 and 630 °C, which belonged to the reduction of Mn_2O_3 to Mn_3O_4 and MnO (*34*). MnO_x/MZI exhibited a strong peak at 541 °C, which originated from excess bulk oxygen in Mn_2O_3 (*34*) and one weak peak at 868 °C, which was responsible for decomposition of the lattice oxygen of Mn_2O_3, forming Mn_3O_4 (*34*). MnO_x/CZI shows two

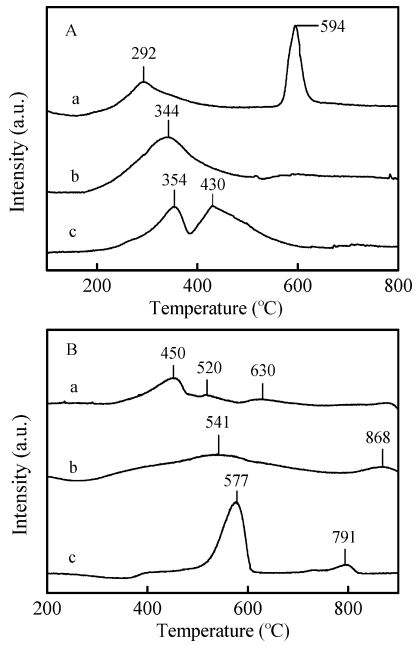

FIGURE 4. TPR profiles (A) and O_2−TPD (B) of different samples: (a) MnO_x/MZIW, (b) MnO_x/MZI, and (c) MnO_x/CZI.

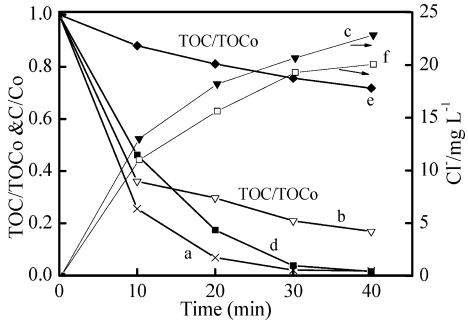

FIGURE 5. Degradation of 2,4-D in the catalytic ozone with MnOx/MZIW: (a) C/C_0, (b) TOC/TOC_0, and (c) Cl^-concentration. The degradation in ozone alone: (d) C/C_0 (e) TOC/TOC_0, (f) Cl^- concentration. (pH 3.7, catalyst: 1.5 g/L, gaseous ozone concentration = 30 mg/L).

weak peaks at 577 and 791 °C, which originated from an excess bulk and the lattice oxygen in Mn_2O_3, respectively. According to TPR and TPD analysis, it was found that the elelctron transfer in MnO_x/MZIW was much easier than that in the other two catalysts, suggesting that MnO_x/MZIW possibly had higher reactivity.

Surface ζ Potential. The activity of solid catalyst in aqueous solution is relative to its surface charge properties. Figure S7 (Supporting Information) shows the changes of the ζ potential with the pH of the solution. The upward shifts of PZC from the 4.9 value for the MZ used as support were observed after the impregnation of Mn. The PZC of MnO_x/MZIW, MnO_x/MZI, and MnO_x/CZI were 5.4, 5.9, and 6.1, respectively. Previous studies (*35*) showed that the negatively charged surface has a strong reactivity toward ozone. This phenomenon is likely the result of the electrophilic characteristics of ozone, which has a high affinity for molecular sites with a strong electronic density.

Ozonation of 2,4-D in the presence of supported MnO_x. The catalytic activity of different catalysts was evaluated by the degradation of 2,4-D with ozone at pH 3.7. As shown in Figure 5, the removal rate of 2,4-D and the formation rate of Cl^- were almost the same, and more than 80% of the total chlorine content was converted into Cl^- ions in the presence

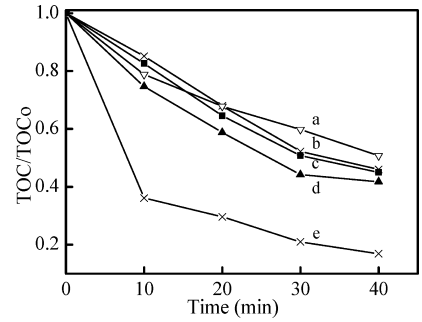

FIGURE 6. Removal of TOC during the degradation of 2,4-D in aqueous dispersions of various catalysts with ozone: (a) MnO_x/CZI, (b) MZ, (c) MnO_x/MZI-2, (d) MnO_x/MZI, and (e) MnO_x/MZIW (pH 3.7, catalyst =1.5 g/L, gaseous ozone concentration = 30 mg/L).

of ozone alone and MnO_x/MZIW with ozone, respectively. However, at a reaction time of 40 min, about 82% of TOC was removed under the latter condition, while only 28% of TOC was removed under the former condition. These results indicated that ozone exhibited similar activity to catalytic ozonation at the stage of dechlorination of 2,4-D, but for the further degradation of 2,4-D, the oxidation performance of ozone was not enough, while the catalytic ozonation using MnO_x/MZIW showed significantly enhanced activity. Therefore, the TOC removal rate was examined to determine the catalytic activity of different catalysts. As shown in Figure 6, MZ, MnO_x/CZI, and MnO_x/MZI-2 (from $Mn(NO_3)_2$) exhibited almost the same catalytic ozonation activity (curves a−c); ∼50% of TOC was removed at a reaction time of 40 min. Compared with these catalysts, MnO_x/MZI showed slightly higher activity; about 60% of TOC was removed (curve d). In contrast, the TOC content of the 2,4-D solution was greatly reduced in MnO_x/MZIW suspension with ozone (curve e). Moreover, according to GC-MS analysis, the residues in the solution after a treatment of 40 min were mainly small molecular organic acids such as glycolic acid and oxalic acid. The aromatic compound was phenol (Table S2, Supporting Information). The TOC of the reaction solution was almost completely removed within 20 min at a 2,4-D concentration of 10 mg/L (Figure S8, Supporting Information). The results demonstrated that MnO_x/MZIW is a highly efficient catalyst for the mineralization of 2,4-D in the ozonation process. Meanwhile, the results indicated that the catalytic activity predominantly depended on the dispersion of MnO_x on the support. The characteristics of CZ led to the lower dispersion of MnO_x and less activity, while the highest dispersion of MnO_x was obtained on MZ (MnO_x/MZIW), leading to the highest activity. On the basis of all the above information, the nature of the support, the preparation method, and the Mn source played a decisive role in the fabrication of the active phases for MnO_x and markedly affected the catalytic activity.

Figure S9 (Supporting Information) presents the temporal variations of TOC content of the 2,4-D solution at various concentrations of MnO_x/MZIW. Clearly, with the concentration of MnO_x/MZIW increasing, the TOC removal rate increased and reached maximum at the catalyst concentration of 2 g/L and then decreased at 3 g/L. The results indicated that there was an optimal dosage of catalyst with a higher concentration leading to catalyst congregation.

The effect of pH on TOC removal is shown in S10 (Supporting Information). The removal rate of TOC was similar in the range of pH 3.7–7 and decreased at pH values higher than 7. The PZC of MnO_x/MZIW was 5.4 pH units, and 2,4-D could be adsorbed onto the catalyst because of its positively charged surface at pH <5.4. On the other hand, ozone reacts readily with the negatively charged surface because of its electrophilic characteristics at pH >5.4.

Therefore, in the range pH 3.7–7, the higher efficiency was attributed to the surface catalytic ozonation. Under alkaline conditions, 2,4-D hardly had any adsorption on the surface of the catalyst, so that it could only react with free •OH in the solution, leading to the lower TOC removal rate.

Reaction Mechanism. The catalytic ozonation mechanism is still controversial because the pathway is so complex, but it is generally believed that, in the heterogeneous catalytic ozonation process, adsorption of ozone and its further decomposition lead to surface bound O radicals and hydroxyl radicals on the surface of catalysts (*36*). To confirm this mechanism, the involved active species were investigated in the catalytic ozonation of 2,4-D. *tert*-Butanol, which is a strong radical scavenger, was adopted as the indicator for the radical type reaction. As shown in Figure S11 (Supporting Information), the addition of *tert*-butanol markedly reduced the ozonation of 2,4-D at pH 7 in the presence of MnO_x/MZIW, indicating that the •OH was the main active species in catalytic ozonation. The results suggested that MnO_x/MZIW accelerated more ozone transformation into •OH radicals. Meanwhile, a series of ozone decomposition experiments were carried out in the presence of the studied catalysts. As shown in Figure S12 (Supporting Information), the ozone decomposition rate was enhanced by different catalysts. MnO_x/CZI showed the least activity (curve c), while the activity of MnO_x/MZI was higher than that of MZ. MnO_x/MZIW exhibited the highest activity (curve e). The ozone decomposition occurred in parallel with the TOC removal in different catalyst suspensions. The results indicated that both MZ and the supported hydrated MnO_x could catalytically decompose O_3 into •OH. According to all the above experiments and previous literature (*2, 21, 37*), a possible mechanism is shown in Table S3 (Supporting Information) for the catalytic ozonation of 2,4-D in MnO_x/MZIW suspension. In this process, first, ozone is trapped by the catalyst and forms surface complex $\equiv MnOH(O_3)_s$ or $\equiv MnO(O_3)_s^-$ on the surface of MnO_x/MZIW. Subsequently, the ozone is catalytically transformed into •OH by MnO_x. The interfacial electron transfer is involved in the catalytic decomposition reaction of ozone. The multivalent MnO_x has two redox couples (Mn^{3+}/Mn^{2+} and Mn^{4+}/Mn^{3+}) to form galvanic cells enhancing the electron transfer, resulting in higher activity for the mineralization of 2,4-D. Therefore, the dispersion and oxidation state of the supported MnO_x were crucial factors for the high efficiency of the catalytic ozonation.

Acknowledgments

This work was supported by the National 863 Project of China (Grant 2006AA06Z307 to Z.G. and 2006AA06Z304 to C.H.) and the National Natural Science Foundation of China (No. 50621804 and 50538090 to J.Q.).

Supporting Information Available

XRD patterns, N_2 adsorption−desorption isotherms, pore-size distribution, XPS Mn 2p spectra, isoelectric points of different samples, UV–vis spectra of the precursor $Mn(CH_3COO)_2 \cdot 4H_2O$ aqueous solution, effects of 2,4-D, catalyst concentrations, and pH on TOC removal, bulk and surface Mn concentrations, GC-MS analysis, a proposed mechanism for the catalytic ozonation of 2,4-D, and O_2−TPD and TPR experiments. This material is available free of charge via the Internet at http://pubs.acs.org.

Literature Cited

(1) Andreozzi, R.; Insola, A.; Carpio, V.; Marotta, R.; Tufano, V. The use of manganese dioxide as a heterogeneous catalyst for oxalic acid ozonation in aqueous solution. *Appl. Catal., A* **1996**, *138*, 75–81.

(2) Legube, B.; Leitner, N. K. V. Catalytic ozonation: A promising advanced oxidation technology for water treatment. *Catal. Today* **1999**, *53*, 61–72.

(3) Lin, S. S.; Gurol, M. D. Catalytic decomposition of hydrogen peroxide on iron oxide: Kinetics, mechanism, and implications. *Environ. Sci. Technol.* **1998**, *32*, 1417–1423.

(4) Dionysiou, D. D.; Suidan, M. T. Effect of ionic strength and hydrogen peroxide on the photocatalytic degradation of 4-chlorophenzoic acid in water. *Appl. Catal., B* **2000**, *26*, 153–171.

(5) Gracia, R.; Cortes, S.; Sarasa, J.; Ormad, P.; Ovelleiro, J. L. TiO_2-catalysed ozonation of raw Ebro river water. *Water Res.* **2000**, *34*, 1525–1532.

(6) Villaseñor, J.; Reyes, P.; Pecchi, G. Catalytic and photocatalytic ozonation of phenol on MnO_2 supported catalysts. *Catal. Today* **2002**, *76*, 121–131.

(7) Cooper, C.; Burch, R. An investigation of catalytic ozonation for the oxidation of halocarbons in drinking water preparation. *Water Res.* **1999**, *33*, 3695–3700.

(8) Hunter, P.; Oyama, S. T. *Control of Volatile Organic Compound Emissions, Conventional and Emerging technologies*; John Wiley and Sons: New York, 2001.

(9) Gervasini, A.; Vezzoli, G. C.; Ragaini, V. VOC removal by synergic effect of combustion catalyst and ozone. *Catal. Today* **1996**, *29*, 449–455.

(10) Kim, S. C. The catalytic oxidation of aromatic hydrocarbons over supported metal oxide. *J. Hazard. Mater.* **2002**, *91*, 285–299.

(11) Huang, W.-J.; Fang, G.-C.; Wang, C.-C. A nanometer-ZnO catalyst to enhance the ozonation of 2,4,6-trichlorophenol in water. *Colloids Surf. A* **2005**, *260*, 45–51.

(12) Han, Y. F.; Chen, F. X.; Zhong, Z. Y.; Ramesh, K.; Chen, L. W.; Widjaja, E. Controlled synthesis, characterization, and catalytic properties of Mn_2O_3 and Mn_3O_4 nanoparticles supported on mesoporous silica SBA-15. *J. Phys. Chem. B* **2006**, *110*, 24450–24456.

(13) Kijlstra, W. S.; Poels, E. K.; Bliek, A. Characterization of Al_2O_3-supported manganese oxides by electron spin resonance and diffuse reflectance spectroscopy. *J. Phys. Chem. B* **1997**, *101*, 309–316.

(14) Brillas, E.; Calpe, J. C.; Cabot, P. L. Degradation of the herbicide 2,4- dichlorophenoxyacetic acid by ozonation catalyzed with Fe^{2+} and UVA light. *Appl. Catal., B* **2003**, *46*, 381–391.

(15) Pignatello, J. Dark and photoassisted Fe^{3+}-catalyzed degradation of chlorophenoxy herbicides by hydrogen peroxide. *Environ. Sci. Technol.* **1992**, *26*, 944–951.

(16) Zepp, R. G.; Faust, B. C.; Hoigne, J. Hydroxyl radical formation in aqueous reactions (pH 3–8) of iron(II) with hydrogen peroxide: the photo-Fenton reaction. *Environ. Sci. Technol.* **1992**, *26*, 313–319.

(17) Trillas, M.; Peral, J.; Domenech, X. Redox photodegradation of 2,4-dichlorophenoxyacetic acid over TiO_2. *Appl. Catal., B: Environ.* **1995**, *5*, 377–387.

(18) Liu, X. L. G.; Yan, Z. Synthesis and stabilization of nanocrystalline zirconia with MSU mesostructure. *J. Phys. Chem. B* **2004**, *108*, 15523–15528.

(19) Blin, J.; Flamant, R.; Su, B. Synthesis of nanostructured mesoporous zirconia using CTMABr-$ZrOCl_2 \cdot 8H_2O$ systems: A kinetic study of synthesis mechanism. *Int. J. Inorg. Mater.* **2001**, *3*, 959–972.

(20) Froba, M.; Kohn, R.; Bouffaud, G.; Richard, O.; van Tendeloo, G. Fe_2O_3 nanoparticles within mesoporous MCM-48 silica: In situ formation and characterization. *Chem. Mater.* **1999**, *11*, 2858–2865.

(21) Kasprzyk-Hordern, B.; Ziółek, M.; Nawrocki, J. Catalytic ozonation and methods of enhancing molecular ozone reactions in water treatment. *Appl. Catal., B* **2003**, *46*, 639–669.

(22) Okamoto, Y.; Kubota, T.; Ohto, Y.; Nasu, S. Metal oxide-support interactions in Fe/ZrO_2 catalysts. *J. Phys. Chem. B* **2000**, *104*, 8462–8470.

(23) Dong, Q.; Zhou, X.; Shao, S. The adsorption behavior of zirconium and iron hydroxides for phosphate. *Ion Exch. Adsorpt.* **2006**, *22*, 363–368.

(24) López, E. F.; Escribano, V. S.; Gallardo-Amores, J. M.; Resini, C.; Busca, G. Structural and morphological characterization of Mn−Zr mixed oxides prepared by a sol−gel method. *Solid State Sci.* **2002**, *4*, 951–961.

(25) Heidt, L. J.; Koster, G. F.; Johnson, A. M. Experimental and crystal field study of the absorption spectrum at 2000 to 8000 Å of manganous perchlorate in aqueous perchloric acid. *J. Am. Chem. Soc.* **1959**, *80*, 6471–6477.

(26) Fabrizioli, P.; Bürgi, T.; Baiker, A. Manganese oxide−silica aerogels: Synthesis and structural and catalytic properties in the selective oxidation of NH_3. *J. Catal.* **2002**, *207*, 88–100.

(27) Qi, G. S.; Yang, R. T. Characterization and FTIR studies of MnO_x−CeO_2 catalyst for low-temperature selective catalytic reduction of NO with NH_3. *J. Phys. Chem. B* **2004**, *108*, 15738–15747.

(28) Velu, S.; Shah, N.; Jyothi, T. M.; Sivasanker, S. Effect of manganese substitution on the physicochemical properties and catalytic toluene oxidation activities of Mg−Al layered double hydroxides. *Microporous Mesoporous Mater.* **1999**, *33*, 61–75.

(29) Dobber, D.; Kiessling, D.; Schmitz, W.; Wendt, G. MnO_x/ZrO_2 catalysts for the total oxidation of methane and chloromethane. *Appl. Catal., B* **2004**, *52*, 135–143.

(30) Arena, F.; Torre, T.; Raimondo, C.; Parmaliana, A. Structure and redox properties of bulk and supported manganese oxide catalysts. *Phys. Chem. Chem. Phys.* **2001**, *3*, 1911–1917.

(31) Koh, D. J.; Chung, J. S.; Kim, Y. G.; Lee, J. S.; Nam, I. S.; Moon, S. H. Structure of Mn−Zr mixed oxide catalysts and their catalytic properties in the CO hydrogenation reaction. *J. Catal.* **1992**, *138*, 630–639.

(32) Stobbe, E. R.; de Boer, B. A.; Geus, J. W. The reduction and oxidation behaviour of manganese oxides. *Catal. Today* **1999**, *47*, 161.

(33) Carno, J.; Ferradon, M.; Bjornbom, E.; Jaras, S. Mixed manganese oxide/platinum catalysts for total oxidation of model gas from wood boilers. *Appl. Catal., A* **1997**, *155*, 265–281.

(34) Luo, M. F.; Yuan, X. X.; Zheng, Z. M. Catalyst characterization and activity of Ag−Mn, Ag−Co, and Ag−Ce composite oxides for oxidation of volatile organic compounds. *Appl. Catal., A* **1998**, *175*, 121–129.

(35) Park, J. S.; Choi, H.; Cho, J. Kinetic decomposition of ozone and *para*-chlorobenzoic acid (pCBA) during catalytic ozonation. *Water Res.* **2004**, *38*, 2285–2292.

(36) Kasprzyk-Hordern, B.; Raczyk-Stanisławiak, U.; wietlik, J.; Nawrocki, J. Catalytic ozonation of natural organic matter on alumina. *Appl. Catal., B* **2006**, *62*, 345–358.

(37) Jung, H.; Choi, H. Catalytic decomposition of ozone and *para*-chlorobenzoic acid (pCBA) in the presence of nanosized ZnO. *Appl. Catal., B* **2006**, *66*, 288–294.

ES0718671